iScience

CellPress
OPEN ACCESS

Article

Effects of hyperhomocysteinemia on follicular development and oocytes quality

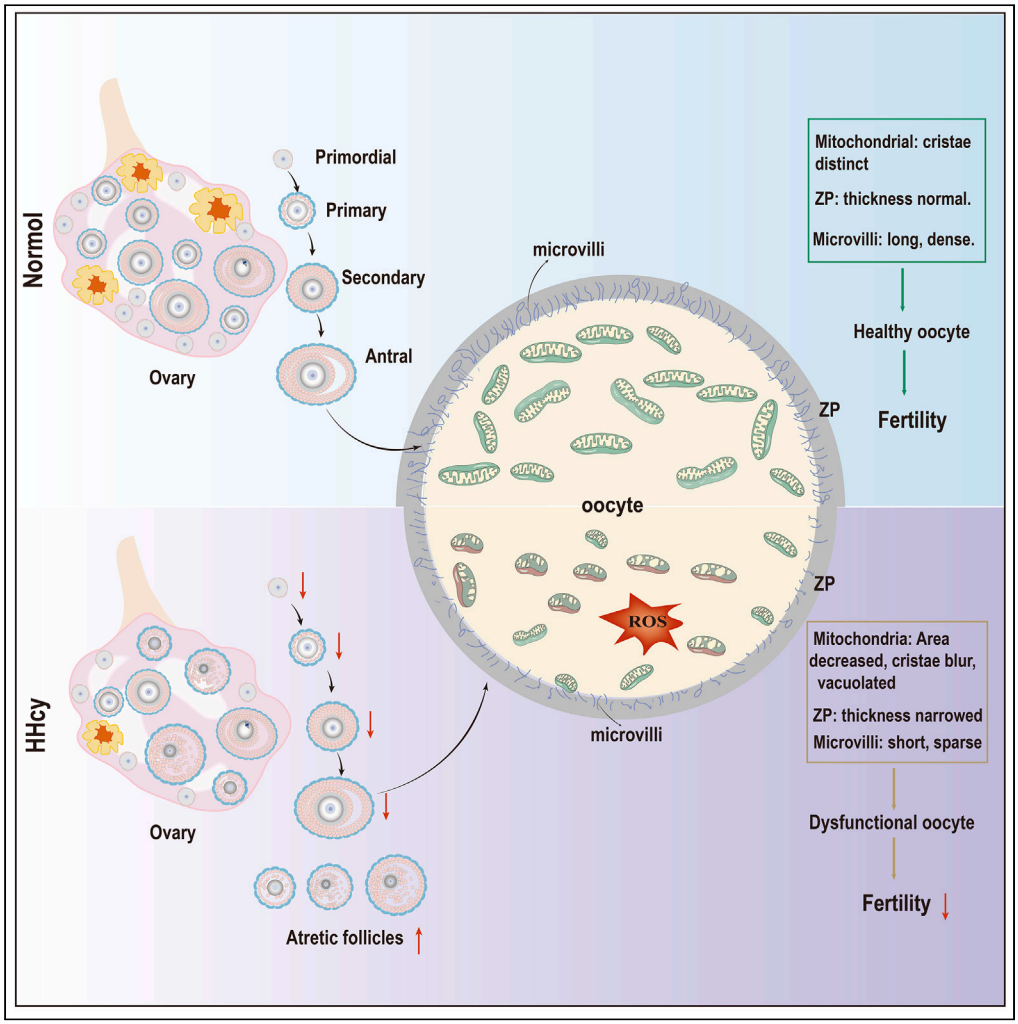

Lu Wang, Jinmei Gao, Jie Ma, ..., Danyu Yang, Jinfang Wang, Rong Hu

hur@nyfy.com.cn

Highlights

Increased atretic follicles and shortened reproductive lifespan in HHcy mice

HHcy causes mitochondrial dysfunction in oocytes

Zona pellucida narrowing and short, sparse microvilli in HHcy mice oocytes

Wang et al., iScience 27, 111241
November 15, 2024
https://doi.org/10.1016/j.isci.2024.111241

iScience

CellPress
OPEN ACCESS

Article

Effects of hyperhomocysteinemia on follicular development and oocytes quality

Lu Wang,[1,7] Jinmei Gao,[1,7] Jie Ma,[1,7] Jing Sun,[2] Yajie Wang,[1] Jia Luo,[6] Zhaoyang Wang,[2] Hui Wang,[3] Jialing Li,[4] Danyu Yang,[1] Jinfang Wang,[5] and Rong Hu[4,6,8,*]

SUMMARY

In patients with polycystic ovary syndrome (PCOS), the concentration of homocysteine (Hcy) in follicular fluid is inversely correlated with oocyte and embryo quality. Nevertheless, other metabolic abnormalities associated with PCOS may also impact oocyte and early embryo quality. Therefore, it remains uncertain whether reproductive function is affected in patients without PCOS with hyperhomocysteinemia (HHcy). Here, we observed reduced fertility, increased ovarian atretic follicles, and reduced oocyte maturation rates in HHcy mice. Proteomic analyses revealed that HHcy causes mitochondrial dysfunction and reduced expression of zona pellucida proteins (ZP1, ZP2, and ZP3) in oocytes. Transmission electron microscopy confirmed abnormal formation of the zona pellucida and microvilli in oocytes from HHcy mice. Additionally, *in vitro* fertilization (IVF) demonstrated a reduction in the rate of 2-cell embryo formation in HHcy mice. These findings reveal that HHcy reduces female reproductive longevity by affecting follicular development and oocyte quality.

INTRODUCTION

Homocysteine (Hcy) is a naturally occurring sulfur-containing amino acid. Insufficient dietary intake of folic acid or vitamin B12, as well as genetic mutations in methylenetetrahydrofolate reductase (MTHFR) and cystathionine-β-synthase (CBS), can lead to abnormal Hcy metabolism.[1,2] This results in elevated levels of Hcy in the body, a condition known as hyperhomocysteinemia (HHcy) when levels exceed 15 μmol/L.[3] Studies have demonstrated that elevated serum Hcy can affect hormone levels and lead to ovulation disorders.[4] Furthermore, increased Hcy levels in the follicular fluid (FF) of patients with polycystic ovary syndrome (PCOS) are significantly correlated with various reproductive problems, including impaired oocyte and embryo quality, birth defects, miscarriage, and low birth weight.[5–9] These findings suggest that elevated Hcy negatively impacts women's reproductive function. In recent years, the incidence of HHcy has been rising due to unhealthy diets and lifestyles, such as excessive alcohol consumption, smoking, and heavy coffee drinking.[10] However, it remains uncertain whether reproductive function is affected in non-PCOS patients with HHcy.

The ovary is the primary functional organ of the female reproductive system, serving two critical physiological roles.[11] First, it is responsible for the maturation and release of oocytes for fertilization. Second, the ovary synthesizes and secretes steroid hormones essential for follicular development and regulating the menstrual/estrous cycle.[12] The follicle, the basic structural and functional unit of the ovary, consists of the oocyte and the surrounding pre-granulosa cells (pre-GCs) or granulosa cells (GCs).[13] Mature oocytes synthesize cytokines, including bone morphogenetic proteins (BMPs) and growth differentiation factor 9 (GDF9), which belong to the transforming growth factor β (TGF-β) family. These cytokines play a crucial role in oocyte development, as well as GC formation and activation.[14,15] Thus, oocyte maturation is essential for follicular development and can be adversely affected by systemic or localized disruptions in the ovarian environment.

Studies have shown that in PCOS patients, Hcy exacerbates autophagy within GCs by manipulating the mammalian target of rapamycin (mTOR) signaling pathway, potentially leading to arrested follicular development and impaired ovulation.[16] Moreover, Hcy impairs porcine oocyte quality via deregulation of one-carbon metabolism, which leads to hypermethylation of mitochondrial DNA and mitochondrial dysfunction.[17] Previous research has primarily examined the impact of elevated Hcy levels in FF of patients with PCOS on the female reproductive system. However, it remains unclear whether reproductive function is similarly affected in non-PCOS patients with HHcy.

In the present study, to investigate the effects of HHcy on female fertility, we established a HHcy mice model and conducted a series of fertility assessments and pathological examinations. Preliminary findings revealed that HHcy mice exhibited reduced litter sizes and a

[1]Ningxia Medical University, General Hospital of Ningxia Medical University, Ningxia, China
[2]Ningxia Medical University, Ningxia, China
[3]Reproductive Medicine Center, Yinchuan Women and Children Healthcare Hospital, Ningxia, China
[4]Reproductive Medicine Center, General Hospital of Ningxia Medical University, Ningxia, China
[5]Department of Obstetrician, General Hospital of Ningxia Medical University, Ningxia, China
[6]Institute of Medical Sciences, General Hospital of Ningxia Medical University, Ningxia, China
[7]These authors contributed equally
[8]Lead contact
*Correspondence: hur@nyfy.com.cn
https://doi.org/10.1016/j.isci.2024.111241

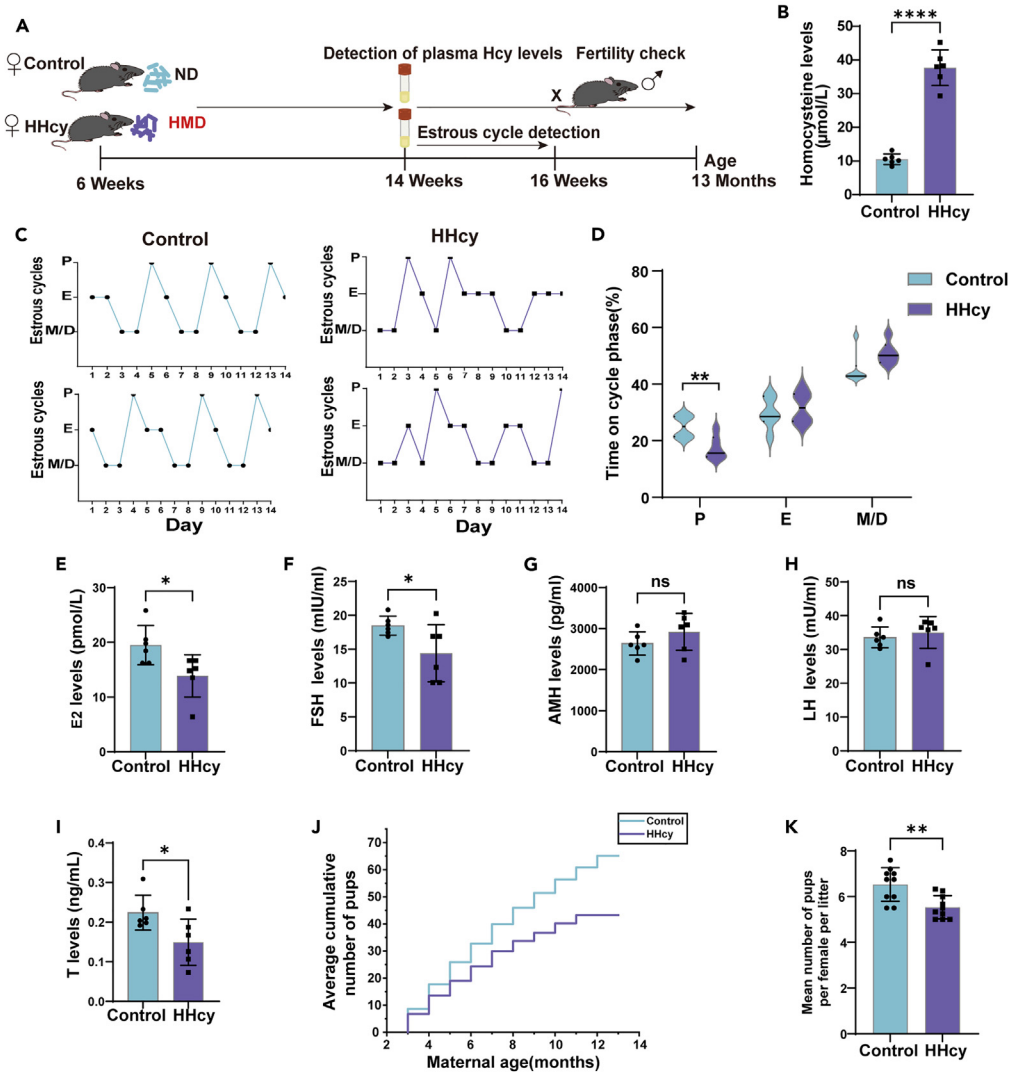

Figure 1. HHcy induced impaired sexual hormone disturbances and reduced fertility in female mice

(A) Schematic illustrating the experimental design (ND: Normal diet, HMD: High-methionine diet).

(B) Serum Hcy levels in mice (n = 6).

(C) Curves of changes in the estrous cycle of female mice in the control and HHcy groups (n = 6) monitored continuously for 14 days.

(D) Ratio of estrous cycle phases (n = 6).

(E–I) The hormone levels of female mice (3 months) in estrus (n = 6.).

(J) Mean cumulative pup numbers for Control (n = 10) and HHcy (n = 10) from 14 weeks to 13 months of age mated with young WT males.

(K) Average number of pups per female per litter (n = 10). Statistical analysis was performed by Student's t-test. Data are represented as mean ± SEM. ns, no significance, *p < 0.05, **p < 0.01, ****p < 0.0001.

significant increase in atretic follicles. Based on these initial data, we hypothesized that HHcy may impair oocyte developmental capacity, leading to decreased fertility, through compromised follicular maturation. To validate our hypothesis and elucidate the underlying mechanisms, we performed comprehensive proteomic analyses of ovarian tissues and conducted subsequent confirmatory experiments. These efforts aim to answer the question of how HHcy leads to reduced fertility in females and provides ideas for the treatment of patients with HHcy infertility.

RESULTS

HHcy induced impaired sexual hormone disturbances and reduced fertility in female mice

To confirm the induction of the HHcy mice model by a high-methionine diet, we examined serum Hcy levels. Compared to the control group, mice fed a high-methionine diet exhibited significantly elevated serum Hcy levels exceeding 15 μmol/L, which meets the diagnostic criteria for HHcy. This indicates that we successfully established a HHcy mice model (Figures 1A and 1B).

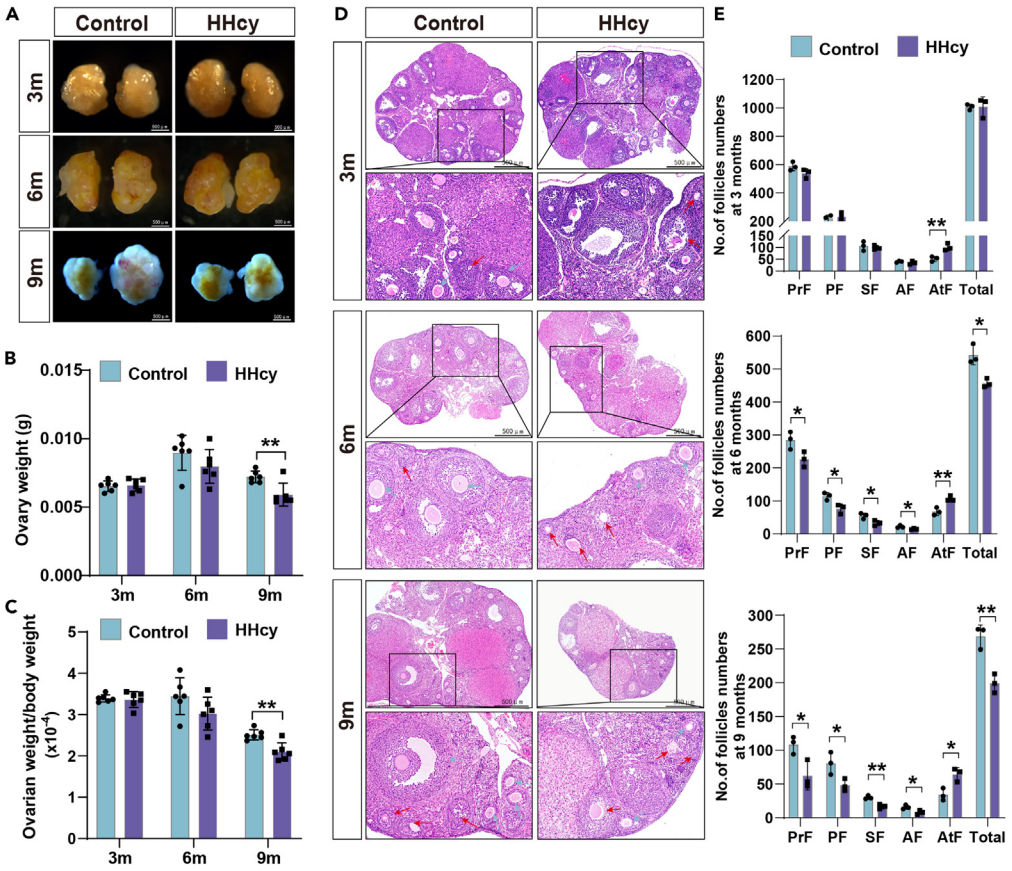

Figure 2. HHcy affects follicular development in female mice

(A) Representative images of ovaries from female mice in 3m, 6m, 9m control, and HHcy groups. Scale bar, 500μm. (The ovarian tissue images of 9-month-old mice appear blue because they were captured using a different method. The ovarian tissues of 3- and 6-month-old mice were photographed under a microscope against black cardstock, while the 9-month-old ovarian tissues were photographed directly on the microscope stage).

(B and C) Ovary weight, ovary weight/body weight of mice in 3M, 6M, 9M control, and HHcy groups ($n = 6$).

(D) H&E staining results showing ovarian histology of Control and HHcy female mice at the indicated ages. Blue arrows indicate healthy follicles, and red arrows indicate atretic follicles. Scale bar, 500μm.

(E) Mean number of primordial follicles (PrF), primary follicles (PF), secondary follicles (SF), antral follicles (AF), atretic follicles (AtF), and total follicles (Total) in the ovaries of control ($n = 3$) and HHcy female mice ($n = 3$). Statistical analysis was performed by Student's t-test. Data are represented as mean ± SEM. *$p < 0.05$, **$p < 0.01$.

The estrous cycle is regulated by rhythmic endocrine interactions between the nervous and reproductive systems, which coordinate the hormonal and ovulatory functions of the ovary.[18] We evaluated the estrous cycle of 3-month-old mice over 14 consecutive days and found that HHcy mice exhibited an irregular estrous cycle (Figures 1C and S1). Additionally, the proportion of time spent in the proestrus was significantly reduced compared with the control group (Figure 1D).

Follicular development and periodic ovulation are regulated by the secretion of sexual hormone.[19] We further investigated the effects of HHcy on serum levels of estradiol (E2), follicle-stimulating hormone (FSH), luteinizing hormone (LH), anti-Mullerian hormone (AMH), and testosterone (T). The HHcy group showed decreased serum levels of E2, FSH, and T, while LH and AMH levels remained unaffected (Figures 1E–1I). After successfully establishing the HHcy mouse model, we conducted a 10-month fertility experiment. Two groups of mice were mated with healthy and fertile male mice (Figure 1A). The results demonstrated a significant reduction in both the cumulative number of offspring and the average number of litters in the HHcy group (Figures 1J and 1K). In conclusion, these results indicate that HHcy induces impaired sex hormone disruption and reduced fertility in female mice.

HHcy leads to increased atretic follicles and decreased age-related ovarian reserve

Follicular development is maintained by the coordination of sex hormones.[11,18] Our studies have demonstrated that HHcy leads to a disorder in sex hormones, which may impact follicular development. Upon examining the ovaries of mice at 3, 6, and 9 months, we observed no notable differences in ovarian size or ovarian index (the ratio of ovarian weight to body weight) between the HHcy and control groups at 3 and 6 months. However, by 9 months, the ovaries of HHcy mice were reduced in size, and the ovarian index was significantly lower (Figures 2A–2C; S2A and S2B).

Histological analysis further revealed that at 3 months, the HHcy group had a comparable number of primordial, primary, secondary, and antral follicles to the control group, but showed an increase in atretic follicles. This distortion in follicular development became more pronounced by 6 and 9 months, with the HHcy group experiencing faster depletion of primordial follicles, a decrease across all follicle stages, and a significant increase in atretic follicles (Figures 2D, 2E and S2C). These findings indicate that HHcy is associated with follicular atresia and an accelerated rate of primordial follicle failure in mice.

HHcy results in a reduction of oocyte developmental potential

In female mammals, fertility is maintained by the regulated development of oocytes and follicles. During follicular development, oocytes not only undergo a sequence of meiotic divisions but also mature into fertilizable eggs.[20] Given that low fertility, abnormal ovarian morphology, and impaired follicular development were observed in HHcy mice, the effects of HHcy on oocyte maturation were investigated in our study. MII oocytes were obtained from the ovaries of 3-month-old and 6-month-old mice following superovulation. Interestingly, the number of MII-stage oocytes obtained from 3-month-old HHcy mice was comparable to that of the control group, but there was a significant reduction in the extrusion of the first polar body (Pb1). However, in 6-month-old mice, both the number of MII oocytes obtained and the rate of Pb1 extrusion were decreased. (Figures 3A–3C; S3).

To further corroborate the impact of HHcy on the maturation process of oocytes, we isolated GV stage oocytes from 3-month-old mice and subjected them to *in vitro* maturation assays (Figure 3D). The results indicated no difference in the count of GV oocytes between HHcy and control groups, yet there was a noteworthy reduction in the rates of germinal vesicle breakdown (GVBD) and Pb1 extrusion within the HHcy group (Figures 3E–3H), echoing the *in vivo* maturation outcomes. Therefore, we conclude that HHcy significantly affects the developmental potential of oocytes.

The proteomic profile analysis of ovarian tissues indicates that HHcy has an impact on ovarian steroidogenesis and its interactions with cumulus cells and zona pellucida

To uncover the mechanism of follicular atresia and diminished oocyte developmental potential arising from HHcy, advanced 4D label-free quantitative proteomics analysis was conducted on ovarian tissues from three 3-month-old mice per group. This analysis successfully quantified 56,611 peptides and identified a total of 5,764 quantifiable proteins. Principal-component analysis (PCA) underscored the exceptional quantitative reproducibility among biological replicates (Figure 4A). Subsequently, differentially expressed proteins (DEPs) were identified (p value <0.05, fold change (FC) > 1.5), revealing 317 upregulated and 113 downregulated proteins (Figures 4B and 4C). An overview of the subcellular localization of these DEPs indicated predominant residency in the cytoplasm (29.07%) and nucleus (21.4%) (Figure 4D). Gene Ontology (GO) term enrichment analysis highlighted their significant involvement in the organization or biogenesis of cellular components, intracellular anatomical structures, organelles, protein binding, and ion binding (Figure 4E). Furthermore, Kyoto Encyclopedia of Genes and Genomes (KEGG) analysis further revealed that, compared to the control group, DEPs in the HHcy mice primarily participate in ovarian steroidogenesis (Figures 4F, S4A and S4B). Reactome pathway analysis revealed that upregulated proteins in the HHcy group predominantly influenced immune regulation, extracellular matrix (ECM) configuration, and cilium assembly (Figures S4C and S4D), and downregulated proteins (mainly ZP1, ZP2, ZP3) were predominantly involved in fertilization, reproduction, and the interaction pathway of cumulus cells with the zona pellucida (ZP) compared to control mice (Figure 4G). Taken together, these findings suggest that impaired follicular development and reduced oocyte developmental potential in HHcy mice may be associated with abnormalities in local immunoregulation of ovarian tissues, organelle assembly, and downregulation of oocyte ZP-related proteins.

HHcy induces mitochondrial dysfunction in oocytes

Our GO enrichment analysis of ovarian tissue proteomics data indicates that HHcy detrimentally affects intracellular structures and organelles within oocytes. Mitochondria, one of the most important organelles in oocytes, increase from dozens to more than a million during oocyte maturation. They not only provide ATP to support oocyte maturation but also regulate calcium homeostasis, apoptosis, and autophagy during oogenesis.[21] Furthermore, after fertilization, paternal mitochondria undergo degradation.[22,23] Thus, the mitochondrial quality of the oocyte directly determines the developmental potential of the oocyte and the quality of the embryo.

Motivated by these considerations, we explored the likelihood that HHcy impairs mitochondrial structure and function. Using transmission electron microscopy (TEM), we examined the mitochondrial structure of oocytes and found abnormal mitochondrial structures in the oocytes of HHcy mice. In the control group, mitochondrial morphology was typical, with clear cristae structures and regular membrane structures. However, the HHcy group exhibited a disappearance of cristae structure and prominent mitochondrial vacuolization (Figure 5A). The results of the statistical analyses demonstrated that the proportion of mitochondria with intact cristae and the mitochondrial area were significantly lower in oocytes from the HHcy group in comparison to the control group (Figures 5B and 5C).

To corroborate the impact of HHcy on mitochondrial functionality in oocytes, we performed Mito Tracker staining. In control oocytes, mitochondrial distribution appeared homogeneous within the cytoplasm. Conversely, HHcy oocytes displayed mitochondrial clumping or areas devoid of mitochondria, with significantly heightened abnormal distribution rates in the HHcy group (Figures 5D and 5E). We further assessed mitochondrial membrane potential ($\Delta\Psi$m) through JC-1 staining, which revealed an increase in JC-1 monomer formation accompanied by a decline in multimer presence in HHcy oocytes. A quantitative portrayal of the aggregate-to-monomer ratio illustrated a substantial diminution in $\Delta\Psi$m in the HHcy group relative to controls (Figures 5F and 5G). Moreover, mitochondrial dysfunction in oocytes induces oxidative stress, leading to the accumulation of reactive oxygen species (ROS), which further negatively affects oocyte quality. Using

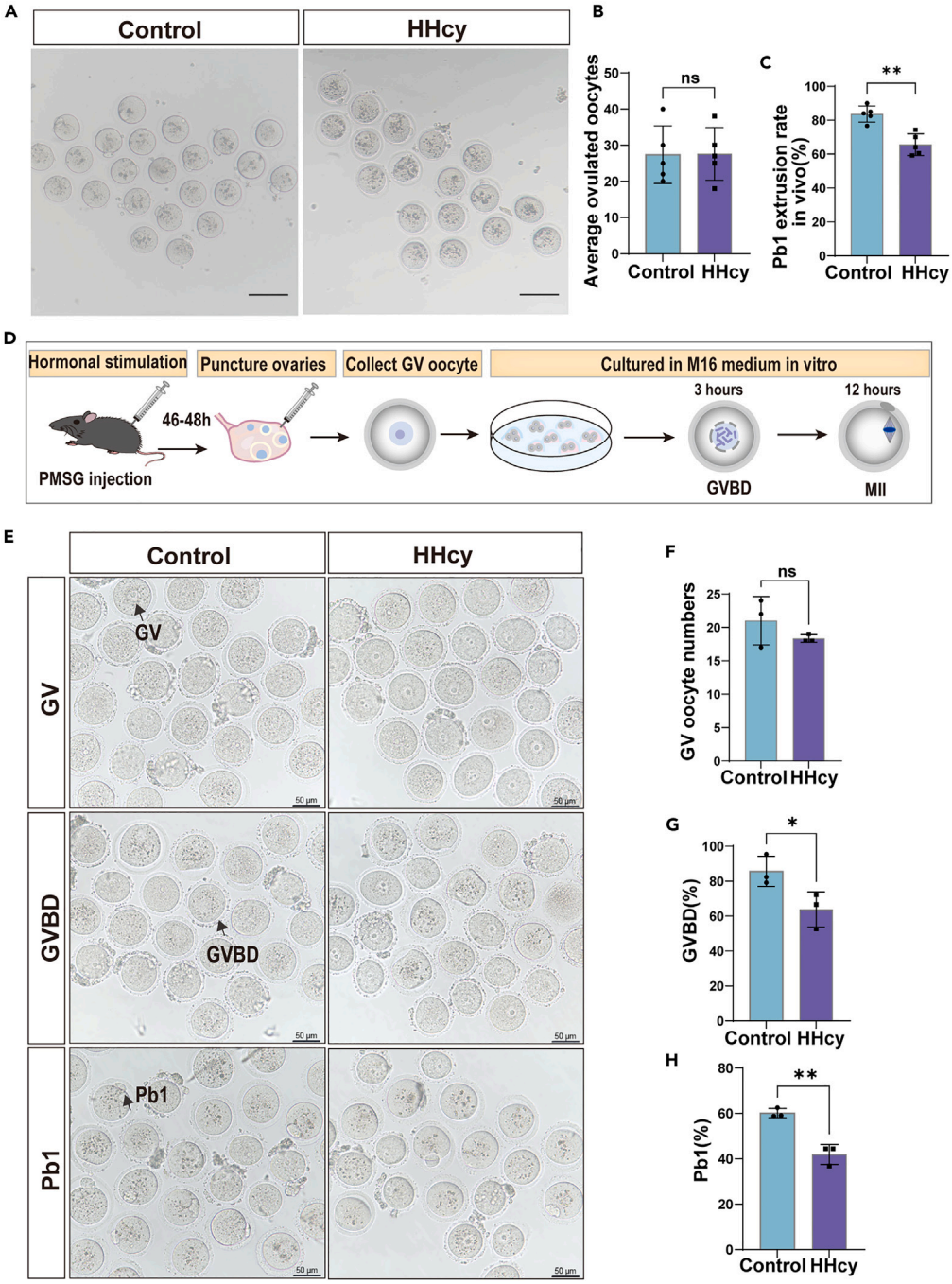

Figure 3. HHcy results in impaired oocyte maturation in mice

(A) Representative images of 3-month-old control and HHcy group MII oocytes. Scale bar, 100μm.

(B) The average number of ovulations in 3-month-old control and HHcy mice (n = 5).

(C) Quantitative analysis of Pb1 extrusion rate in control and HHcy oocytes (n = 5).

(D) Schematic diagram of the workflow for *in vitro* oocyte culture.

(E) Bright-field images of control and HHcy group oocytes during *in vitro* culture maturation with arrows pointing to GV, GVBD, and Pb1 oocytes. Scale bar, 50μm.

(F–H) GV oocyte acquisition and percentage of GVBD, Pb1(n = 3). Statistical analysis was performed by Student's t-test. Data are represented as mean ± SEM. ns, no significance, *$p < 0.05$, **$p < 0.01$.

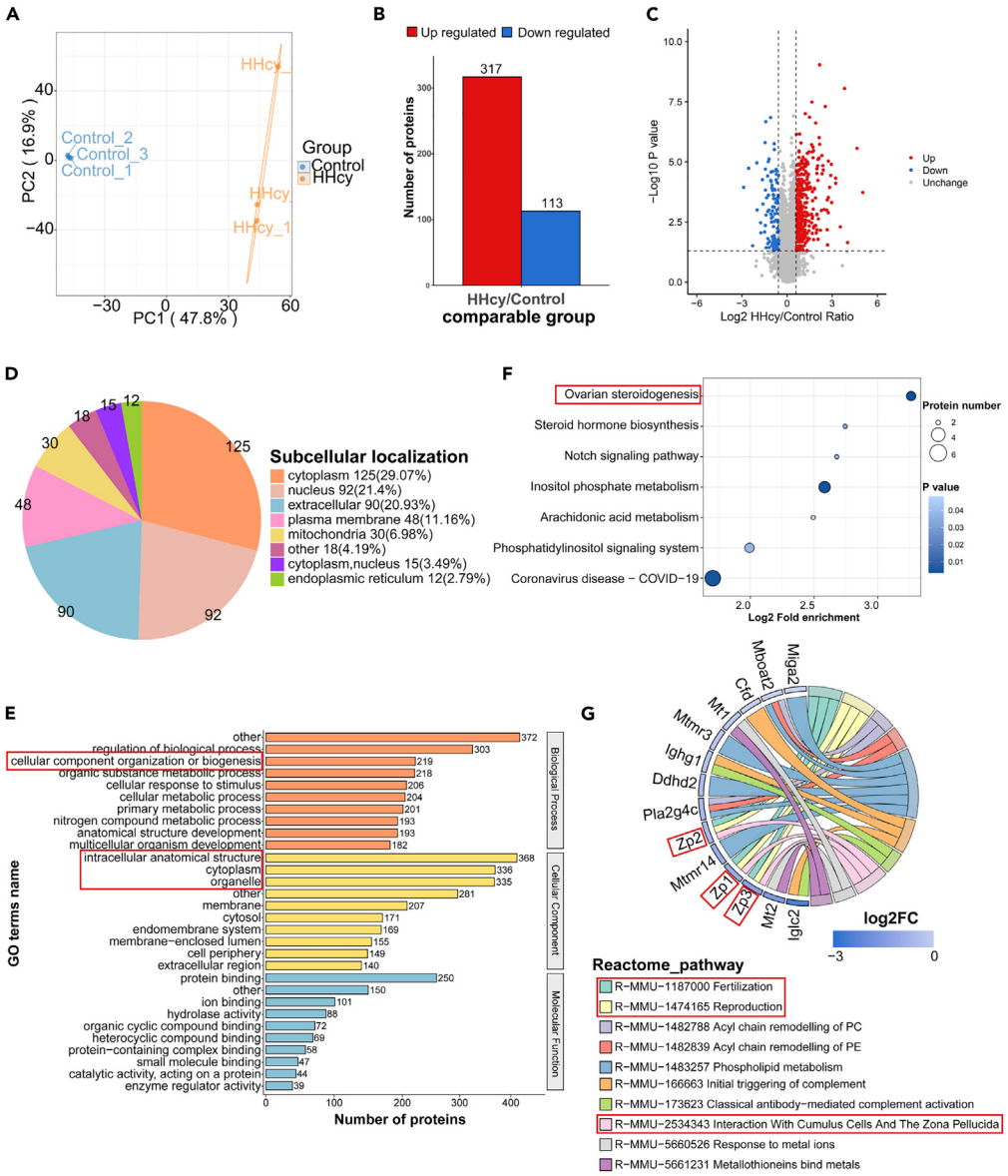

Figure 4. Proteomic analysis of mice ovarian tissue

(A) Principal component analysis of protein expression patterns in Control and HHcy Groups (n = 3).

(B and C) DEGs of control and HHcy mouse ovarian tissues through LC-MS/MS (Significantly (Fold Change, FC > 1.5) up- and down (Fold Change, FC < 1/1.5) -regulated.

(D) Diagram of protein distribution among subcellular compartments.

(E) GO annotation analysis of the identified proteins was performed using eggnog-mapper software (v2.1.6) based on the EggNOG database.

(F) KEGG pathway enrichment analysis of control and HHcy group mouse ovary LC-MS/MS data.

(G) Reactome pathway analysis of downregulated DEPs in control and HHcy group mouse ovary LC-MS/MS data.

DCFH-DA (2,7-dichlorofluorescin diacetate) staining, we ascertained ROS levels within oocytes. HHcy oocytes manifested elevated ROS increased, as indicated by heightened fluorescence intensity compared to the control group (Figures 5H and 5I). In summary, these results suggest that HHcy leads to a reduction in oocyte quality through the induction of mitochondrial structural abnormalities and dysfunction.

HHcy induces abnormal formation of zona pellucida and microvilli in mouse oocytes

Proteomic analysis revealed that ZP proteins (ZP1, ZP2, and ZP3) were significantly downregulated in the HHcy group (Figure 4G). ZP proteins play a crucial role in various reproductive processes, including oogenesis, fertilization, and pre-implantation. These processes involve

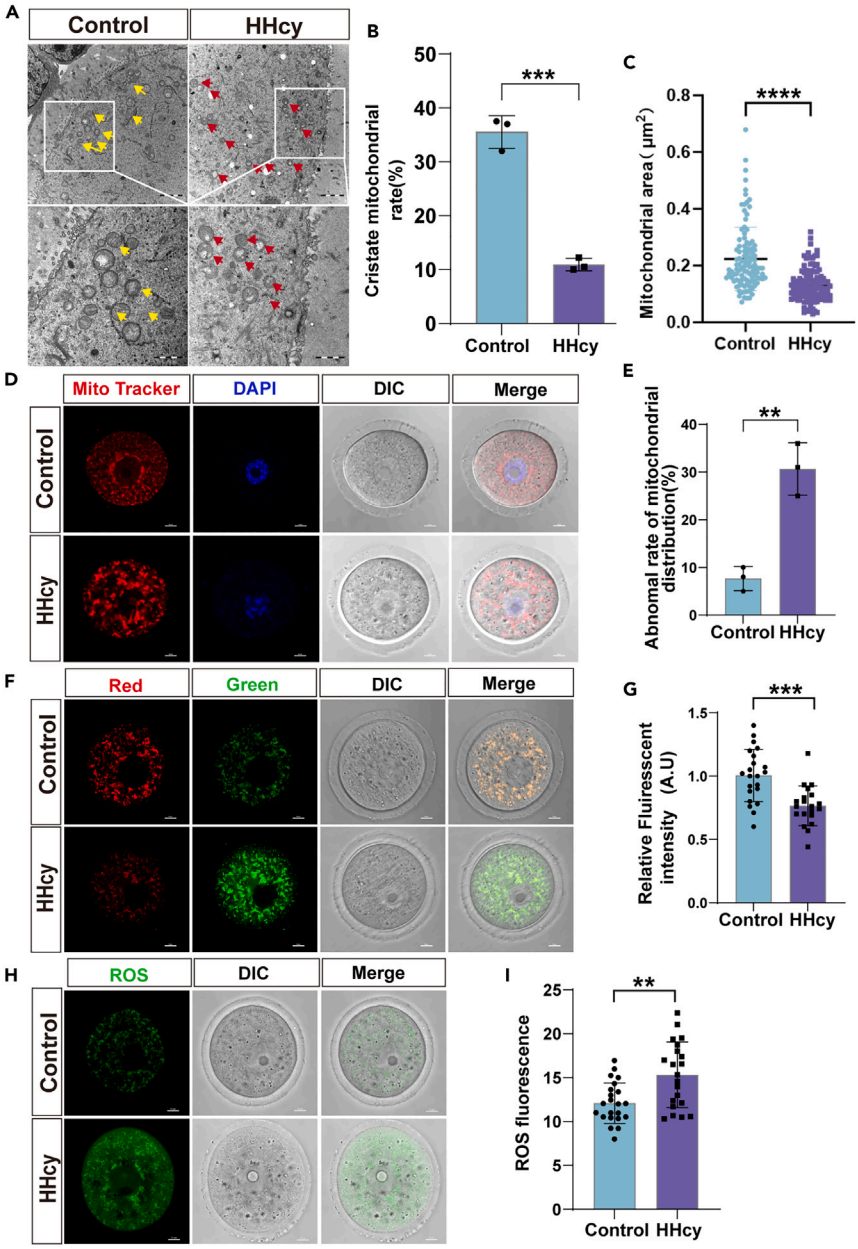

Figure 5. HHcy affects mitochondrial function in oocytes

(A) TEM images of oocytes in ovarian tissues (n = 3). Yellow arrows represent cristate mitochondria, and red arrows represent fuzzy mitochondrial cristae and vacuolated mitochondria. Scale bar, 1 μm. Scale for enlarging images, 2 μm.

(B) The ratio of cristae mitochondria in control and HHcy oocytes was observed in TEM images (n = 3).

(C) Mitochondrial area was calculated in control (n = 109) and HHcy (n = 117) group oocytes observed in TEM images.

(D) Representative images of mitochondrial distribution in control and HHcy oocytes. Oocytes were stained with Mito Tracker Red to show mitochondria. Scale bar, 10 μm.

(E) The abnormal rate of mitochondrial distribution was recorded in control and HHcy oocytes.

(F) Representative images of JC-1 kit staining in control and HHcy groups oocytes. Scale bar, 10 μm.

(G) The ratio of red to green fluorescence intensity was calculated in control (n = 22) and HHcy (n = 20) oocytes.

(H) Representative images of DCFH-DA staining in control and HHcy groups. Scale bar, 10 μm.

(I) Fluorescent intensity of ROS was analyzed in control (n = 23) and HHcy (n = 21) oocytes. Statistical analysis was performed by Student's t-test. Data are represented as mean ± SEM. $^{**}p < 0.01$, $^{***}p < 0.001$, $^{****}p < 0.0001$.

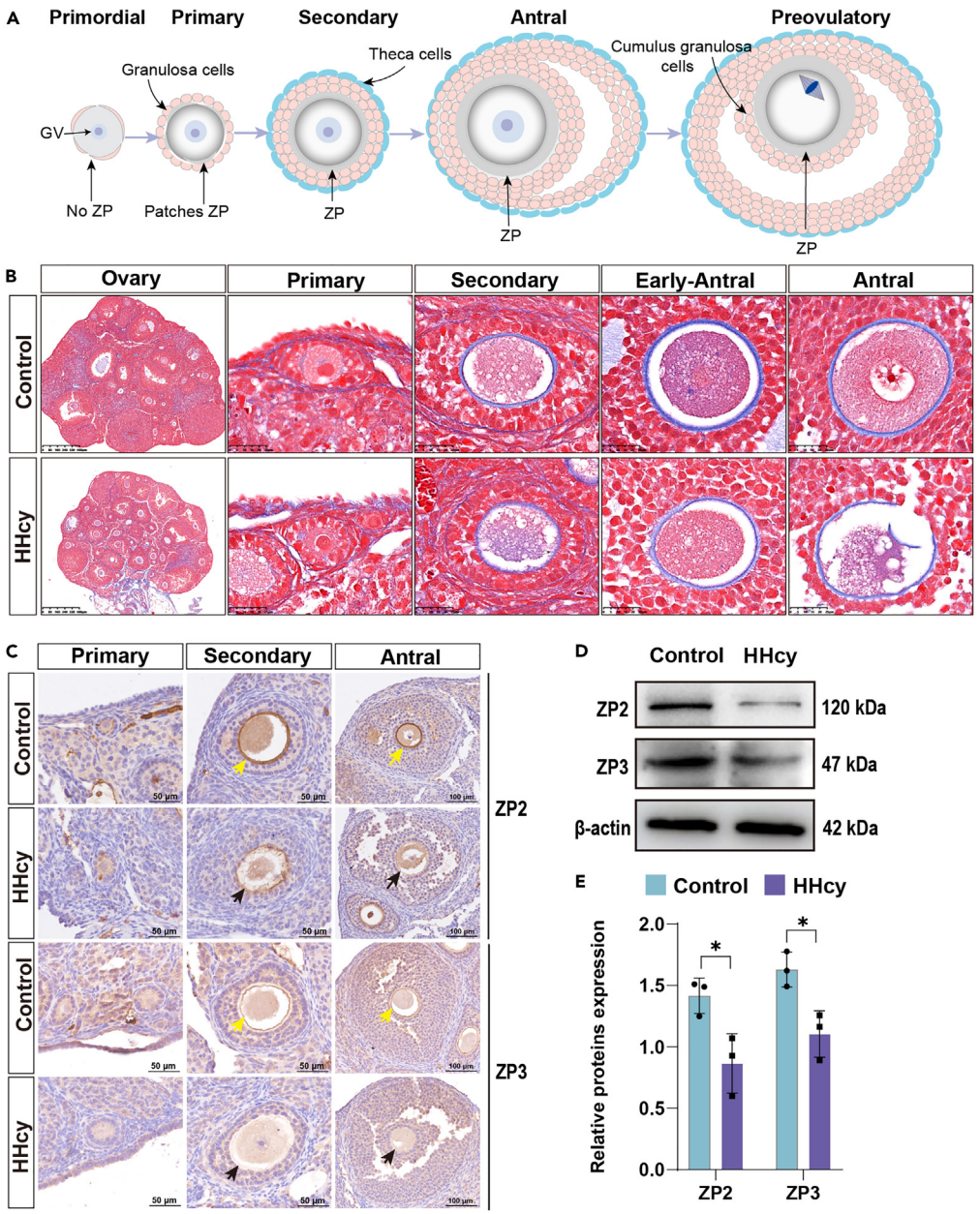

Figure 6. The expression of ZP proteins decreased in female mice with HHcy

(A) Schematic representation of ZP production during oocyte growth in mice.

(B) Masson staining for changes in the fibrils of follicular ZP at all levels in the ovaries of control and HHcy mice ($n = 3$). Arrows indicate the presence of fibrils: yellow arrows indicate the formation of normal ZP fibrils, and black arrows indicate abnormal formation of ZP fibrils. Scale for whole ovary image, 400μm. Scale for follicle images, 25μm.

(C) Immunohistochemical detection of ZP2 and ZP3 protein expression in control and HHcy oocytes ($n = 3$). Arrow indicates the location of ZP. Scale for primary and secondary follicle images, 50μm. Scale for antral follicle images, 100μm.

(D) Western blot probing with anti-ZP2 and anti-ZP3 of oocytes from control and HHcy female mice.

(E) Quantitative analysis of ZP2 and ZP3 protein expression in control and HHcy groups. Statistical analysis was performed by Student's t-test. Data are represented as mean ± SEM ($n = 3$). *$p < 0.05$.

promoting oocyte and follicle health during egg formation, providing a species-specific binding site for sperm during fertilization, preventing polyspermy, and protecting the embryo as it travels through the female reproductive tract to the uterus.[24] Non-growing oocytes, less than 12 μm in diameter (0.9 pL in volume), initially lack ZP, which begins to envelop the oocyte surface in diffuse fibrils as growth commences (Figure 6A). These fibrils subsequently condense to form a robust and uniform ECM.[25,26]

To investigate whether HHcy disrupts oocyte ZP formation by downregulating ZP protein expression, we initially evaluated ECM expression via Masson staining. Results indicated reduced expression of fibrils in primary, secondary, and antral follicles in the HHcy group compared to the control group (Figure 6B). Given that ZP is involved in the entire follicular development process, we hypothesized that HHcy impairs follicular development by inducing abnormal oocyte ZP formation. We screened genes expressed specifically at each stage of follicular development and analyzed them alongside proteomic data. We observed downregulation of ZP1, ZP2, ZP3, Ybx2, Padi6, and Ooep among proteins expressed specifically during primary follicular development. During secondary follicle development, Gpd1 was upregulated and Ybx2 was downregulated (Figure S5).

Further analysis showed that HHcy leads to alterations in proteins specific to each stage of follicular development, impairing overall follicular development. Mouse and human ZP genes are encoded by single-copy genes located on different chromosomes and are highly expressed in the ovary by growing oocytes during late stages of oogenesis.[27,28] To further validate the information obtained from DEPs, we analyzed alterations in oocyte ZP2 and ZP3 at all follicular stages and found diminished expression of ZP proteins in oocytes from the HHcy group at all stages (Figure 6C). Western blotting demonstrated a reduction in the levels of ZP2 and ZP3 in oocytes derived from HHcy mice in comparison to oocytes from control mice. (Figures 6D and 6E). Accordingly, elevated Hcy interferes with ZP formation primarily through a reduction in ZP protein levels, leading to impaired follicular development.

In addition, the content of ZP protein was positively correlated with its structural thickness.[29] We assessed the ZP thickness of secondary, antral, and preovulatory follicles of comparable sizes using ovarian tissue TEM. The ZP of oocytes in the HHcy group was significantly thinner than that in the control group (Figures 7A–7F). Notably, we observed significant differences in oocyte microvilli. Statistical analysis revealed that, compared with the control group, the microvilli density of oocytes in the HHcy group decreased and their length was reduced (Figures 7G and 7H). Microvilli are conserved structures in the ZP that are essential for communication between oocytes and GCs, promoting normal follicle formation.[30] Furthermore, microvilli are known to facilitate membrane fusion between somatic cells and gametes during fertilization.[31] They likely provide a scaffold for the presentation of adhesion and fusion proteins.[32] Therefore, we investigated whether the abnormal formation of oocyte ZP and microvilli caused by HHcy affected fertilization. Our results showed that the 2-cell embryo rate was significantly lower in the HHcy group (Figures 7I and 7J). These findings suggest that the abnormal formation of oocyte ZP and microvilli is another major cause of reduced fertility in HHcy female mice.

DISCUSSION

In the present study, we established a female mouse model of HHcy and found that fertility was reduced, atretic follicles were increased, and the developmental potential of oocytes was decreased. Through comprehensive 4D label-free quantitative proteomic analysis of ovarian tissue and subsequent validation experiments, it was demonstrated that HHcy led to mitochondrial dysfunction in oocytes. Moreover, our data convincingly showed that HHcy distorted the typical formation of the ZP and oocyte microvilli in female mice, this led to impaired follicular development and decreased oocyte quality, which in turn affects fertilization and embryonic development. In conclusion, our study demonstrates that HHcy reduces fertility and shortens reproductive life in female mice.

Previous studies have shown that elevated FF Hcy is associated with conditions such as diminished ovarian reserve (DOR), premature ovarian insufficiency (POI) and infertility.[33] Furthermore, a recent study indicates that elevated levels of Hcy may result in impaired ovulatory function.[4] We thus posit that reduced ovulation in HHcy-afflicted female mice could be attributed to the onset of DOR. Our data demonstrated that at 3 months, there was a notable increase in atretic follicles in HHcy female mice compared to controls. However, by 6 and 9 months of age, a marked decline in follicles across all stages was evident. Several clinical studies have found a negative correlation between FF Hcy levels and oocyte and embryo quality.[7,9] This association prompted us to investigate whether HHcy leads to reduced oocyte quality. Although the number of oocytes post-ovulation in 3-month-old HHcy mice was similar to control groups, their quality was evidently compromised. These observations support the notion that HHcy-induced deterioration of oocyte quality is a principal factor in fertility disorders in mice.

Mitochondria provide energy to support transcription and translation during oocyte maturation, fertilization, and early embryonic development. Thus, mitochondrial dysfunction is a key factor responsible for chromosomal anomalies during the meiotic divisions of mammalian oocytes.[34,35] In the present study, we found abnormal mitochondrial structure of oocytes in the HHcy group, evidenced by reduced mitochondrial area, blurred mitochondrial cristae, and severe vacuolization. Additionally, the mitochondrial distribution in HHcy oocytes was abnormal, and the mitochondrial membrane potential was reduced, indicating impaired mitochondrial function. Mitochondria are the primary source of ROS during intracellular oxidative phosphorylation (OXPHOS).[36,37] In HHcy mouse oocytes, an accumulation of ROS suggested HHcy-induced oxidative stress, which might be the trigger for oocyte damage. This observation aligns with findings that Hcy exposure induced ROS overproduction, impairing porcine oocyte developmental capacity.[17] In conclusion, our data confirm that HHcy generates oxidative stress by inducing mitochondrial dysfunction, which obstructs oocyte development.

The mammalian egg ZP consists of a specific set of proteins. It comprises three proteins (ZP1-3) in mice, with ZP4 as an additional protein in humans. ZP2 and ZP3 are found in approximately equal amounts within the ZP of both mice and humans, with lesser quantities of ZP1 and ZP4.[38–40] It is established that female mice deficient in ZP1 ($ZP1^{-/-}$) retain their fertility, although with lower fecundity compared to wild-type counterparts, attributed to an increased early loss of preimplantation embryos within the oviduct.[41] The presence of ZP2 and ZP3 in oocytes grown in $ZP1^{-/-}$ mice supports the formation of heterodimers that can assemble into elongated fibrils. However, in the absence of ZP1, these fibrils fail to form stable cross-links, making the embryo more vulnerable as it transitions from the oviduct to the uterus. Female mice homozygous null for either ZP2 ($ZP2^{-/-}$) or ZP3 ($ZP3^{-/-}$) produce eggs that lack a ZP, rendering them completely infertile,[42–44] suggesting the

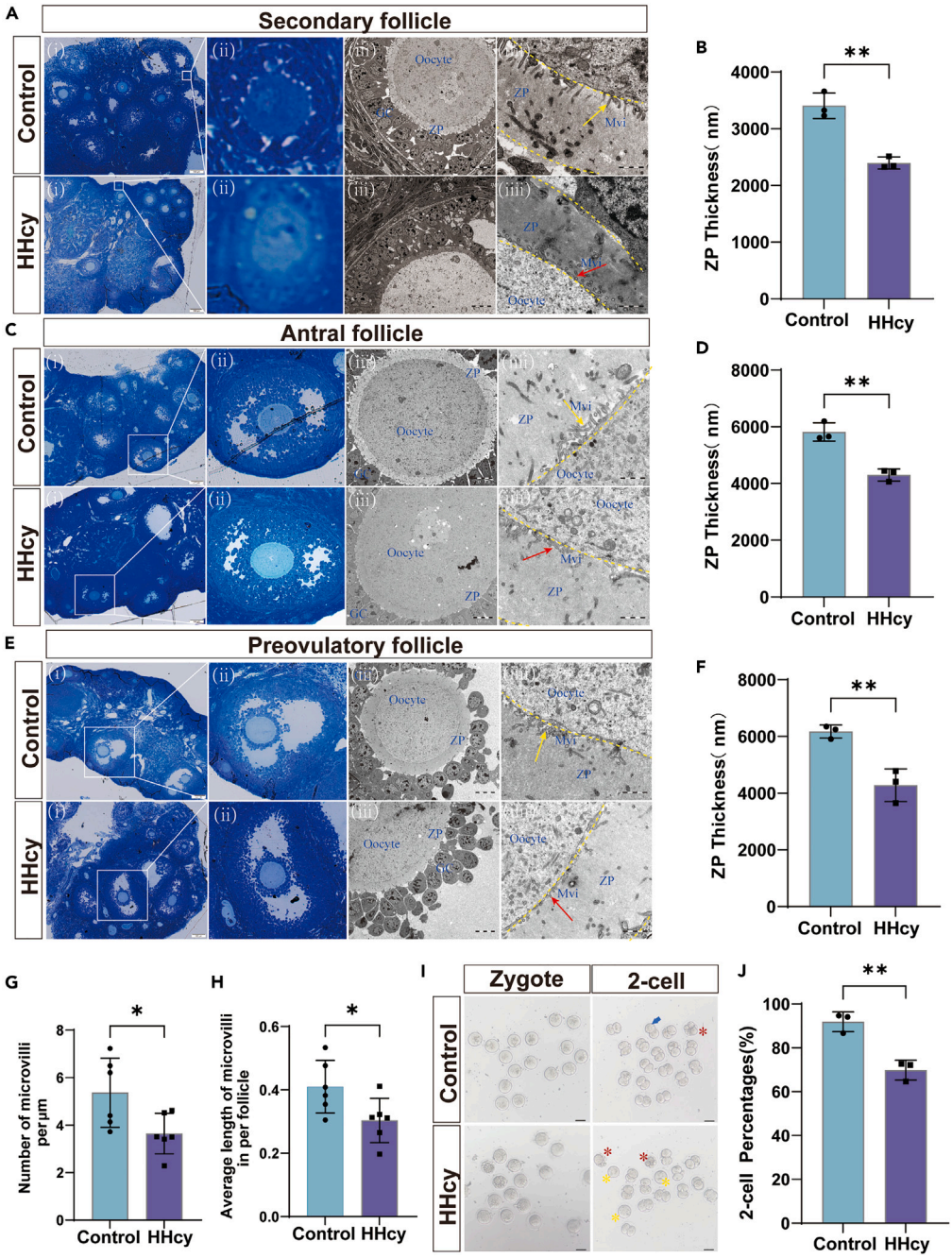

Figure 7. Changes in oocyte ZP and microvilli

(A, C, and E) TEM of oocyte ZP thickness and microvilli morphology in secondary, antral and preovulatory follicles. (i, ii are the localization and magnification of antral follicles selected for TEM observation of ZP and microvilli, respectively. iii, iiii are the TEM images of similar size antral follicles in the control and HHcy groups. The yellow dashed portion is the oocyte ZP. Yellow arrows indicate the normal microvilli morphology and density, and red arrows indicate the microvilli with abnormal morphology and density). Scale bar for i, 100μm. iii, Scale bar, 10μm. And iiii, Scale bar, 1μm.

(B, D, and F) Oocyte ZP thickness in secondary, antral and preovulatory follicles ($n = 3$).

(G) The density of oocyte microvilli in each follicle ($n = 6$).

(H) The average length of oocyte microvilli in each follicle ($n = 6$).

(I) Shown are representative brightfield images of zygote and 2-cell stage embryos. Blue arrows indicate normally developing embryos, red asterisks indicate cytoplasmic fragmentation, and yellow asterisks indicate unfertilized eggs or developmentally arrested embryos. Scale bar, 50 μm.

(J) Percentage of 2-cell embryos ($n = 3$). Statistical analysis was performed by Student's t-test. Data are represented as mean ± SEM. *$p < 0.05$, **$p < 0.01$.

indispensability of ZP2 and ZP3 for ZP assembly around growing oocytes. In the present study, it was found that the protein expression of ZP1, ZP2, and ZP3 was downregulated in oocytes of HHcy mice. Additionally, the zona pellucida was thinner in secondary follicles, antral follicles, and preovulatory follicles of similar size compared to those in the control group.

The ZP's viscous matrix is posited to stabilize the interconnected network formed by gap junctions, bridging the microvilli of the oocyte and the transzonal projections (TZPs) from accompanying GCs.[45] The oocyte's surface microvilli are typically evenly distributed with an average length of 1.06 $\pm$ 0.09 μm. When the oocyte TZPs approaches the surface of the oocyte, they are coupled with one long microvillus and surrounded by 5–6 short microvilli.[46,47] Unexpectedly, our findings indicated a reduction in the length and density of microvilli on oocytes from HHcy mice during follicle development. Therefore, we speculate that fertilization and embryonic development disorders due to abnormal formation of ZP and microvilli may be an important factor in the decline of oocyte quality in HHcy mice. Obviously, our data show that HHcy leads to a decrease in 2-cell embryo formation rate. Surprisingly, the study found that female mice heterozygous null for ZP3 ($ZP3^{+/-}$) have a thin ZP (width $\approx$2.7 $\pm$ 1.2 μm) compared to the ZP of eggs from wild-type females (width $\approx$6.2 $\pm$ 1.9 μm), but are as fertile as wild-type females.[48] Therefore, ZP width is not a critical parameter for sperm binding to the ZP or fertilization, however, it may affect oocyte quality or the process of embryo implantation.

Here, we discovered that HHcy disrupts ovarian follicle and oocyte development by compromising mitochondrial function in oocytes and the architecture of TZPs. Nevertheless, the underlying mechanisms by which HHcy induces anomalies in microvillus formation pose an intriguing scientific question for future inquiry. To summarize, our work lays a robust theoretical groundwork for investigating the molecular dynamics of how HHcy influences oocyte maturation. More importantly, our findings provide insights into the occurrence of infertility due to clinical HHcy.

Limitations of the study

In this study, the effects of HHcy on follicular development and oocyte quality were investigated mainly using a mouse model. Although it has been proven that the decrease in oocyte quality in mice due to HHcy may be associated with structural changes and dysfunction of oocyte mitochondria and abnormal formation of oocyte zona pellucida and microvilli. Further studies are required to investigate the specific mechanisms by which HHcy leads to abnormal microvillus formation in oocytes. Unfortunately, we were unable to find ZP1 antibody with good specificity, such that we are missing validation of ZP1 in ovarian tissue and oocytes. In addition, we failed to obtain oocyte samples from normal controls and infertile patients in the clinic. In future studies, we will investigate the molecular mechanism by which HHcy leads to the abnormal formation of microvilli in oocytes and collect relevant clinical samples for experiments to identify key therapeutic targets for the HHcy-induced infertility.

RESOURCE AVAILABILITY

Lead contact

Further information and requests for resources and reagents should be directed to and will be fulfilled by the lead contact, Rong Hu (hur@nyfy.com.cn).

Materials availability

This study did not generate any new material.

Data and code availability

- Raw proteomic data have been deposited to the ProteomeXchange via the PRIDE and are publicly available as of the date of publication. Accession numbers are listed in the key resources table.
- This paper does not report original code.
- Any additional information required to reanalyze the data reported in this paper is available from the lead contact upon request.

ACKNOWLEDGMENTS

We thank Ningxia Key Laboratory of Clinical Pathogenic Microorganisms, Stem Cell Research Institute, General Hospital of Ningxia Medical University, Ningxia, China, and State Key Laboratory of Agrobiotechnology, College of Biological Sciences, China Agricultural University, Beijing, China. Last but not least, we highly appreciate all the participants in our study.

Funding: National Natural Science Foundation of China (grant number: 82160293 to R.H.), Key Research and Development Program of Ningxia Hui Autonomous Region (grant number: 2022CMG02028 to R.H.), Ningxia Hui Autonomous Region Natural Science Foundation (grant number: 2022AAC02060 to R.H.).

AUTHOR CONTRIBUTIONS

Conceptualization: R.H. and L.W.; methodology: L.W., J.G., J.M., J.S., and Y.W.; investigation: L.W., J.M., J.S., Y.W., and J.L.; visualization: L.W., J.G., Z.W., H.W., J.Li., J.M., D.Y., and J.W.; supervision: R.H.; writing (original draft): L.W.; writing (review and editing): R.H. and L.W.; funding acquisition: R.H. All authors read and approved the final version of the revised manuscript.

DECLARATION OF INTERESTS

The authors declare that they have no competing interests.

STAR★METHODS

Detailed methods are provided in the online version of this paper and include the following:

- KEY RESOURCES TABLE
- EXPERIMENTAL MODEL AND STUDY PARTICIPANT DETAILS
  - Animals
- METHOD DETAILS
  - Serum Hcy and hormone levels determination
  - Estrus cycle examination
  - Fertility test
  - Oocyte isolation and *in vitro* maturation
  - Histological analysis of ovaries
  - Quantitative proteomics analysis
  - Active mitochondrial staining
  - Assay of mitochondrial membrane potential
  - ROS detection
  - Immunohistochemistry
  - Transmission electron microscopy (TEM)
  - Western blot analysis
  - *In vitro* fertilization and embryo culture
- QUANTIFICATION AND STATISTICAL ANALYSIS

SUPPLEMENTAL INFORMATION

Supplemental information can be found online at https://doi.org/10.1016/j.isci.2024.111241.

Received: April 4, 2024
Revised: June 12, 2024
Accepted: October 21, 2024
Published: October 23, 2024

REFERENCES

1. Tripathi, M., Singh, B.K., Zhou, J., Tikno, K., Widjaja, A., Sandireddy, R., Arul, K., Abdul Ghani, S.A.B., Bee, G.G.B., Wong, K.A., et al. (2022). Vitamin B(12) and folate decrease inflammation and fibrosis in NASH by preventing syntaxin 17 homocysteinylation. J. Hepatol. *77*, 1246–1255. https://doi.org/10.1016/j.jhep.2022.06.033.
2. Hou, N., Chen, S., Chen, F., Jiang, M., Zhang, J., Yang, Y., Zhu, B., Bai, X., Hu, Y., Huang, H., and Xu, C. (2016). Association between premature ovarian failure, polymorphisms in MTHFR and MTRR genes and serum homocysteine concentration. Reprod. Biomed. Online *32*, 407–413. https://doi.org/10.1016/j.rbmo.2016.01.009.
3. Moll, S., and Varga, E.A. (2015). Homocysteine and MTHFR Mutations. Circulation *132*, e6–e9. https://doi.org/10.1161/circulationaha.114.013311.
4. Michels, K.A., Wactawski-Wende, J., Mills, J.L., Schliep, K.C., Gaskins, A.J., Yeung, E.H., Kim, K., Plowden, T.C., Sjaarda, L.A., Chaljub, E.N., and Mumford, S.L. (2017). Folate, homocysteine and the ovarian cycle among healthy regularly menstruating women. Hum. Reprod. *32*, 1743–1750. https://doi.org/10.1093/humrep/dex233.
5. Vujkovic, M., de Vries, J.H., Dohle, G.R., Bonsel, G.J., Lindemans, J., Macklon, N.S., van der Spek, P.J., Steegers, E.A.P., and Steegers-Theunissen, R.P.M. (2009). Associations between dietary patterns and semen quality in men undergoing IVF/ICSI treatment. Hum. Reprod. *24*, 1304–1312. https://doi.org/10.1093/humrep/dep024.
6. Ebisch, I.M.W., Peters, W.H.M., Thomas, C.M.G., Wetzels, A.M.M., Peer, P.G.M., and Steegers-Theunissen, R.P.M. (2006). Homocysteine, glutathione and related thiols affect fertility parameters in the (sub)fertile couple. Hum. Reprod. *21*, 1725–1733. https://doi.org/10.1093/humrep/del081.
7. Berker, B., Kaya, C., Aytac, R., and Satiroglu, H. (2009). Homocysteine concentrations in follicular fluid are associated with poor oocyte and embryo qualities in polycystic ovary syndrome patients undergoing assisted reproduction. Hum. Reprod. *24*, 2293–2302. https://doi.org/10.1093/humrep/dep069.
8. Chang, H., Xie, L., Ge, H., Wu, Q., Wen, Y., Zhang, D., Zhang, Y., Ma, H., Gao, J., Wang, C.C., et al. (2019). Effects of hyperhomocysteinaemia and metabolic syndrome on reproduction in women with polycystic ovary syndrome: a secondary analysis. Reprod. Biomed. Online *38*, 990–998. https://doi.org/10.1016/j.rbmo.2018.12.046.
9. Ocal, P., Ersoylu, B., Cepni, I., Guralp, O., Atakul, N., Irez, T., and Idil, M. (2012). The association between homocysteine in the follicular fluid with embryo quality and pregnancy rate in assisted reproductive techniques. J. Assist. Reprod. Genet. *29*, 299–304. https://doi.org/10.1007/s10815-012-9709-y.
10. Zeng, Y., Li, F.F., Yuan, S.Q., Tang, H.K., Zhou, J.H., He, Q.Y., Baker, J.S., Dong, Y.H., and Yang, Y.D. (2021). Prevalence of Hyperhomocysteinemia in China: An Updated Meta-Analysis. Biology *10*, 959. https://doi.org/10.3390/biology10100959.
11. McGee, E.A., and Hsueh, A.J. (2000). Initial and cyclic recruitment of ovarian follicles. Endocr. Rev. *21*, 200–214. https://doi.org/10.1210/edrv.21.2.0394.
12. Hsueh, A.J.W., Kawamura, K., Cheng, Y., and Fauser, B.C.J.M. (2015). Intraovarian control of early folliculogenesis. Endocr. Rev. *36*, 1–24. https://doi.org/10.1210/er.2014-1020.
13. Maheshwari, A., and Fowler, P.A. (2008). Primordial follicular assembly in humans–revisited. Zygote *16*, 285–296. https://doi.org/10.1017/s0967199408004802.
14. Chang, H.M., Qiao, J., and Leung, P.C.K. (2016). Oocyte-somatic cell interactions in the human ovary-novel role of bone morphogenetic proteins and growth differentiation factors. Hum. Reprod. Update *23*, 1–18. https://doi.org/10.1093/humupd/dmw039.
15. Knight, P.G., and Glister, C. (2006). TGF-beta superfamily members and ovarian follicle development. Reproduction *132*, 191–206. https://doi.org/10.1530/rep.1.01074.
16. Li, T., Dong, G., Kang, Y., Zhang, M., Sheng, X., Wang, Z., Liu, Y., Kong, N., and Sun, H. (2022). Increased homocysteine regulated by androgen activates autophagy by suppressing the mammalian target of rapamycin pathway in the granulosa cells of polycystic ovary syndrome mice. Bioengineered *13*, 10875–10888. https://doi.org/10.1080/21655979.2022.2066608.
17. Jia, L., Zeng, Y., Hu, Y., Liu, J., Yin, C., Niu, Y., Wang, C., Li, J., Jia, Y., Hong, J., and Zhao, R. (2019). Homocysteine impairs porcine oocyte quality via deregulation of one-carbon metabolism and hypermethylation of mitochondrial DNA. Biol. Reprod. *100*, 907–916. https://doi.org/10.1093/biolre/ioy238.
18. Morris, M.E., Meinsohn, M.C., Chauvin, M., Saatcioglu, H.D., Kashiwagi, A., Sicher, N.A., Nguyen, N., Yuan, S., Stavely, R., Hyun, M., et al. (2022). A single-cell atlas of the cycling murine ovary. Elife *11*, e77239. https://doi.org/10.7554/eLife.77239.
19. Fiorentino, G., Cimadomo, D., Innocenti, F., Soscia, D., Vaiarelli, A., Ubaldi, F.M., Gennarelli, G., Garagna, S., Rienzi, L., and

Zuccotti, M. (2023). Biomechanical forces and signals operating in the ovary during folliculogenesis and their dysregulation: implications for fertility. Hum. Reprod. Update *29*, 1–23. https://doi.org/10.1093/humupd/dmac031.

20. Gilchrist, R.B., Lane, M., and Thompson, J.G. (2008). Oocyte-secreted factors: regulators of cumulus cell function and oocyte quality. Hum. Reprod. Update *14*, 159–177. https://doi.org/10.1093/humupd/dmm040.
21. May-Panloup, P., Boucret, L., Chao de la Barca, J.M., Desquiret-Dumas, V., Ferré-L'Hotellier, V., Morinière, C., Descamps, P., Procaccio, V., and Reynier, P. (2016). Ovarian ageing: the role of mitochondria in oocytes and follicles. Hum. Reprod. Update *22*, 725–743. https://doi.org/10.1093/humupd/dmw028.
22. Van Blerkom, J. (2011). Mitochondrial function in the human oocyte and embryo and their role in developmental competence. Mitochondrion *11*, 797–813. https://doi.org/10.1016/j.mito.2010.09.012.
23. Larsson, N.G., Wang, J., Wilhelmsson, H., Oldfors, A., Rustin, P., Lewandoski, M., Barsh, G.S., and Clayton, D.A. (1998). Mitochondrial transcription factor A is necessary for mtDNA maintenance and embryogenesis in mice. Nat. Genet. *18*, 231–236. https://doi.org/10.1038/ng0398-231.
24. Wassarman, P.M., and Litscher, E.S. (2021). Zona Pellucida Genes and Proteins: Essential Players in Mammalian Oogenesis and Fertility. Genes *12*, 1266. https://doi.org/10.3390/genes12081266.
25. Wassarman, P.M., and Mortillo, S. (1991). Structure of the mouse egg extracellular coat, the zona pellucida. Int. Rev. Cytol. *130*, 85–110. https://doi.org/10.1016/s0074-7696(08)61502-8.
26. Greve, J.M., and Wassarman, P.M. (1985). Mouse egg extracellular coat is a matrix of interconnected filaments possessing a structural repeat. J. Mol. Biol. *181*, 253–264. https://doi.org/10.1016/0022-2836(85)90089-0.
27. Liang, L.F., Chamow, S.M., and Dean, J. (1990). Oocyte-specific expression of mouse Zp-2: developmental regulation of the zona pellucida genes. Mol. Cell Biol. *10*, 1507–1515. https://doi.org/10.1128/mcb.10.4.1507-1515.1990.
28. Epifano, O., Liang, L.F., Familari, M., Moos, M.C., Jr., and Dean, J. (1995). Coordinate expression of the three zona pellucida genes during mouse oogenesis. Development *121*, 1947–1956. https://doi.org/10.1242/dev.121.7.1947.
29. Litscher, E.S., and Wassarman, P.M. (2020). Zona Pellucida Proteins, Fibrils, and Matrix. Annu. Rev. Biochem. *89*, 695–715. https://doi.org/10.1146/annurev-biochem-011520-105310.
30. Li, R., and Albertini, D.F. (2013). The road to maturation: somatic cell interaction and self-organization of the mammalian oocyte. Nat. Rev. Mol. Cell Biol. *14*, 141–152. https://doi.org/10.1038/nrm3531.
31. Runge, K.E., Evans, J.E., He, Z.Y., Gupta, S., McDonald, K.L., Stahlberg, H., Primakoff, P., and Myles, D.G. (2007). Oocyte CD9 is enriched on the microvillar membrane and required for normal microvillar shape and distribution. Dev. Biol. *304*, 317–325. https://doi.org/10.1016/j.ydbio.2006.12.041.
32. Wilson, N.F., and Snell, W.J. (1998). Microvilli and cell-cell fusion during fertilization. Trends Cell Biol. *8*, 93–96. https://doi.org/10.1016/s0962-8924(98)01234-3.
33. Lu, Y., and Xia, Z. (2023). Diminished ovarian reserve is associated with metabolic disturbances and hyperhomocysteinemia in women with infertility. J. Obstet. Gynaecol. *43*, 2282722. https://doi.org/10.1080/01443615.2023.2282722.
34. Tesarik, J., and Mendoza-Tesarik, R. (2023). Mitochondria in Human Fertility and Infertility. Int. J. Mol. Sci. *24*, 8950. https://doi.org/10.3390/ijms24108950.
35. Mikwar, M., MacFarlane, A.J., and Marchetti, F. (2020). Mechanisms of oocyte aneuploidy associated with advanced maternal age. Mutation research. Mutat. Res. Rev. Mutat. Res. *785*, 108320. https://doi.org/10.1016/j.mrrev.2020.108320.
36. Waltz, F., and Giegé, P. (2020). Striking Diversity of Mitochondria-Specific Translation Processes across Eukaryotes. Trends Biochem. Sci. *45*, 149–162. https://doi.org/10.1016/j.tibs.2019.10.004.
37. Nohl, H., Gille, L., and Staniek, K. (2005). Intracellular generation of reactive oxygen species by mitochondria. Biochem. Pharmacol. *69*, 719–723. https://doi.org/10.1016/j.bcp.2004.12.002.
38. Jovine, L., Darie, C.C., Litscher, E.S., and Wassarman, P.M. (2005). Zona pellucida domain proteins. Annu. Rev. Biochem. *74*, 83–114. https://doi.org/10.1146/annurev.biochem.74.082803.133039.
39. Goudet, G., Mugnier, S., Callebaut, I., and Monget, P. (2008). Phylogenetic analysis and identification of pseudogenes reveal a progressive loss of zona pellucida genes during evolution of vertebrates. Biol. Reprod. *78*, 796–806. https://doi.org/10.1095/biolreprod.107.064568.
40. Szymański, W., and Kazdepka-Ziemińska, A. (2003). [Effect of homocysteine concentration in follicular fluid on a degree of oocyte maturity]. Ginekol. Pol. *74*, 1392–1396.
41. Rankin, T., Talbot, P., Lee, E., and Dean, J. (1999). Abnormal zonae pellucidae in mice lacking ZP1 result in early embryonic loss. Development *126*, 3847–3855. https://doi.org/10.1242/dev.126.17.3847.
42. Rankin, T.L., O'Brien, M., Lee, E., Wigglesworth, K., Eppig, J., and Dean, J. (2001). Defective zonae pellucidae in Zp2-null mice disrupt folliculogenesis, fertility and development. Development *128*, 1119–1126. https://doi.org/10.1242/dev.128.7.1119.
43. Rankin, T., Familari, M., Lee, E., Ginsberg, A., Dwyer, N., Blanchette-Mackie, J., Drago, J., Westphal, H., and Dean, J. (1996). Mice homozygous for an insertional mutation in the Zp3 gene lack a zona pellucida and are infertile. Development *122*, 2903–2910. https://doi.org/10.1242/dev.122.9.2903.
44. Liu, C., Litscher, E.S., Mortillo, S., Sakai, Y., Kinloch, R.A., Stewart, C.L., and Wassarman, P.M. (1996). Targeted disruption of the mZP3 gene results in production of eggs lacking a zona pellucida and infertility in female mice. Proc. Natl. Acad. Sci. USA *93*, 5431–5436. https://doi.org/10.1073/pnas.93.11.5431.
45. Jaffe, L.A., and Egbert, J.R. (2017). Regulation of Mammalian Oocyte Meiosis by Intercellular Communication Within the Ovarian Follicle. Annu. Rev. Physiol. *79*, 237–260. https://doi.org/10.1146/annurev-physiol-022516-034102.
46. Baena, V., and Terasaki, M. (2019). Three-dimensional organization of transzonal projections and other cytoplasmic extensions in the mouse ovarian follicle. Sci. Rep. *9*, 1262. https://doi.org/10.1038/s41598-018-37766-2.
47. El-Hayek, S., Yang, Q., Abbassi, L., FitzHarris, G., and Clarke, H.J. (2018). Mammalian Oocytes Locally Remodel Follicular Architecture to Provide the Foundation for Germline-Soma Communication. Curr. Biol. *28*, 1124–1131.e3. https://doi.org/10.1016/j.cub.2018.02.039.
48. Wassarman, P.M., Qi, H., and Litscher, E.S. (1997). Mutant female mice carrying a single mZP3 allele produce eggs with a thin zona pellucida, but reproduce normally. Proc. Biol. Sci. *264*, 323–328. https://doi.org/10.1098/rspb.1997.0046.

STAR★METHODS

KEY RESOURCES TABLE

REAGENT or RESOURCE	SOURCE	IDENTIFIER
Antibodies		
STAR Polyclonal antibody	Proteintech	Cat# 12225-1-AP; RRID: AB_2115832
Anti-HSD17B7 antibody	Invitrogen	Catalog#PA5120533; RRID: AB_2914105
CYP17A1 Recombinant Rabbit Monoclonal Antibody	Invitrogen	Cat#MA5-35632 RRID: AB_2849532
Rabbit polyclonal antibody to ZP2	Abmart	Cat#PA5354; RRID:AB_3665051
ZP3 Polyclonal antibody	Proteintech	Cat#21279-1-AP; RRID : AB_11124319
Beta Actin Recombinant antibody	Proteintech	Cat#81115-1-RR; RRID : AB_2923704
Goat anti-rabbit IgG	Invitrogen	Cat#31460; RRID: AB_228341
Chemicals, peptides, and recombinant proteins		
Serum gonadotropin for injection (PMSG)	Ningbo Second Hormone Company	Cat#110254564
Human chorionic gonadotropin (hCG)	Ningbo Second Hormone Company	Cat#110251282
Hyaluronidase digestion	Nanjing Aibei Biotechnology Co., Ltd.	Cat#M2215
Hoechst 33342	Sigma-Aldrich	Cat#B2261
4%Paraformaldehyde	Beyotime	Cat#P0099
M2 medium	Sigma-Aldrich	Cat#M7167
M16 medium	Sigma-Aldrich	Cat#M7292
Mineral oil	Sigma-Aldrich	Cat#M5310
Masson trichrome staining	Beyotime	Cat#C0189S
MitoTracker® Red CMXRos	Cell Signaling,	Cat#9082
MitoProbe JC-1 Assay Kit	KeyGEN BioTECH,	Cat#KGA1904-100
DCFH-DA	Nanjing Jiancheng Bioengineering Institute,	Cat#E004-1-1
HTF medium	Nanjing Aibei Biotechnology Co., Ltd.	Cat#M1135
KSOM medium	Nanjing Aibei Biotechnology Co., Ltd.	Cat#M1435
Deposited data		
Raw proteomic data	This paper	PRIDE: PXD053081
Software and algorithms		
GraphPad Prism software	N/A	GraphPad Prism 10
ImageJ	N/A'	ImageJ (https://imagej.net/)
eggnog-mapper (V2.0)	N/A	http://eggnog-mapper.embl.de
PSORTb (V3.0)	N/A	WoLF PSORT: Protein Subcellular Localization Prediction (hgc.jp)

EXPERIMENTAL MODEL AND STUDY PARTICIPANT DETAILS

Animals

This study was conducted in strict accordance with the ethical standards set forth by the Ningxia Medical University's Animal Ethics Committee and all processes were carried out according to the Animal Research guidelines (Approval no.: IACUC-2024-013).

The female and male mice (C57BL/6J) were obtained from the Laboratory Animal Center of Ningxia Medical University (Ningxia, China). All experimental mice were housed under specific pathogen-free (SPF) conditions at 24 ± 1°C, with 40–70% humidity, and a 12-h light/dark cycle. They were provided with food and water *ad libitum*. The six-week-old female mice were randomly assigned to either the control group or the HHcy group. The control group was provided with a standard diet, whereas the HHcy group was fed a diet containing 3% methionine, sourced from Komitsu Yutai (Beijing, China). Following an eight-week feeding period, serum samples were collected and the HHcy mouse models were confirmed by measuring serum Hcy levels. HHcy was defined as Hcy concentrations of 15 μmol/L or higher.

METHOD DETAILS

Serum Hcy and hormone levels determination

Mice were injected intraperitoneally with 4% chloral hydrate and blood was gained from the eyeballs, The collected blood was kept at room temperature for 2 h and centrifuged at 4°C for 10 min at 3000 rpm. The supernatant was collected, and the serum Hcy concentration of the mice was measured using the Homocysteine (Enzyme Cycling Assay) Test Kit (JL-T1120, JONLN, China). The serum levels of estradiol (E2), follicle stimulating hormone (FSH), luteinizing hormone (LH), anti-Müllerian hormone (AMH) and testosterone (T) were determined by enzyme-linked immunosorbent assay (ELISA) kit (JL11790-96T, JL10239-96T, JL10432-96T, JL20476-96T, JONLN and E-OSEL-M0003, Elabscience).

Estrus cycle examination

The mice underwent daily vaginal exfoliated cell smears from 17:30 to 18:00. 20 μL of saline was gently placed on the vaginal opening and rinsed 2–3 times. The rinsing solution was then coated on slides and observed under a light microscope. Mice estrous cycle was determined by the morphology and type of exfoliated cells for 14 days of observation. Proestrus (P) is characterized by predominantly nucleated epithelial cells, while estrus (E) is characterized by predominantly keratinized and non-nucleated epithelial cells. Metestrus (M) is characterized by a mixture of nucleated epithelial cells, keratinized and non-nucleated epithelial cells, and neutrophils. Diestrus (D) is characterized by a large number of neutrophils.

Fertility test

Female 14 weeks old mice (n = 10 in each group) were mated with normal adult males (female to male ratio = 2:1). Successful mating was determined by vaginal plugs on the second day of mating, the number of mice in each litter was recorded at birth. At three weeks of age, the litters were separated from females and males were introduced for mating purposes, this experiment continued for 10 months. After the experiment, we recorded the total number of litters and the average number of litters per mouse.

Oocyte isolation and *in vitro* maturation

MII collection: 14-week-old female mice were injected with 5 IU PMSG (Ningbo Second Hormone Company, 110254564), and 48 h later with 5 IU hCG (Ningbo Second Hormone Company, 110251282). After 13.5 h, cumulus-oocyte complexes (COCs) were obtained from the oviducts and MII oocytes were collected by removing the cumulus cells using hyaluronidase digestion (Nanjing Aibei Biotechnology Co., Ltd., M2215).

GV oocytes collection and culture: 14-week-old female mice were injected intraperitoneally with 5 IU PMSG. After 48 h, ovarian tissues were obtained to acquire GV oocytes under stereo microscope, the GV oocytes were then cultured with M16 medium (Sigma-Aldrich, M7292) under mineral oil at 37°C, 5% CO2.

Histological analysis of ovaries

Ovarian tissues were harvested from 3-month-old, 6-month-old, and 9-month-old proestrus mice and fixed with 4% paraformaldehyde (PFA) (Beyotime, P0099, China) overnight. Ovarian tissues were then dehydrated with ethanol and cleared within xylene. Finally, cleared Ovarian tissues were embedded in paraffin and sectioned serially at 5 μm thickness to produce paraffin section of ovarian tissue. Following deparaffinization with xylene and graded ethanol solutions, hematoxylin and eosin (H&E) staining was performed to observe ovarian follicle morphologic changes and count follicle numbers. To perform follicle counting, all follicles were counted from the first cross-section through the last for each ovary and only the follicles with clear oocyte nuclei in the ovaries were counted to avoid double counting. The counting of follicles at different stages of development followed the established standards set by Pedersen and Peters. The total number of follicles per ovary was determined by adding up all the counted sections of the whole ovary without a correction factor applied. Masson trichrome staining (Beyotime, C0189S, China) was used to detect zona pellucida fibrils, following the manufacturer's instructions.

Quantitative proteomics analysis

The 4D-label-free-based quantitative proteomic analysis of mice ovary was carried out by Jingjie PTM Biolabs Inc. (Hangzhou, China). Protein was extracted from ovarian tissues of three mice per group, and the protein concentration was determined using a BCA kit following the manufacturer's instructions. After the proteins were cleaved into peptides using trypsin, the peptides were desalted by the C18 SPE column. The peptides were subjected to a series of treatments followed by the timsTOF Pro (Bruker Daltonics) mass spectrometry. Next, we used PSORTb

software (v3.0) to predict and analyze the subcellular structure of the proteins. The DEPs were classified by pathway using Gene Ontology (GO) analysis and Kyoto Encyclopedia of the Genome (KEGG). Additionally, the DEPs were analyzed for GO classification, KEGG pathway and Reactome pathway functional enrichment.

Active mitochondrial staining

MitoTracker Red CMXRos (Cell Signaling, 9082) was used to label the mitochondria detect active mitochondrion in oocyte. Oocytes were cultured in M16 culture medium containing 200 nM MitoTracker Red CMXRos at 37°C and 5% CO2 for 30 min. After being washed three times with M2 medium, the mitochondria of oocytes were imaged using laser confocal microscopy.

Assay of mitochondrial membrane potential

Mitochondrial membrane potential was evaluated using MitoProbe JC-1 Assay Kit (KeyGEN BioTECH, KGA1904-100). A 2 mM JC-1 working solution was prepared in M16 medium. Oocytes were then incubated with JC-1 working solution at 37°C and 5% CO_2 for 20 min. Then, washed them twice with Incubation Buffer, and imaged immediately using a confocal laser microscope.

ROS detection

ROS levels were detected in oocytes using the DCFH-DA (2,7-Dichlorofluorescin Diacetate) probe, following the manufacturer's instructions (Nanjing Jiancheng Bioengineering Institute, E004-1-1). Briefly, after the oocytes were incubated in DCFH-DA working solution at 37°C for 20 min and washed twice with (phosphate-buffered saline) PBS, the ROS fluorescence signals in oocytes were collected using a Nikon A1 laser scanning confocal microscope.

Immunohistochemistry

Ovarian tissues were fixed in 4% PFA overnight, embedded in paraffin, and sectioned at 5 μm. After dewaxing and rehydration, then, paraffin sections of ovarian tissue were boiled at high temperature for 5 min and low temperature for 15 min in 0.01 M sodium citrate for antigen retrieval. Next cover the tissues with 3% H_2O_2, incubate them at room temperature in the absence of light for 10 min, and rinse them with PBS three times for 5 min each. After that the tissue sections were closed in TBS containing 3% BSA for 30 min. Subsequently, the sections were incubated overnight at 4°C with specific primary antibodies, including anti-ZP2 and anti-ZP3. Sections were washed three times with PBS for 5 min each. It was then stain with HRP-conjugated secondary antibody (Zhong Shan Jin Qiao, ZB-2306) for 30 min at 37°C. The sections' color was developed with 3, 3'- diaminobenzidine (DAB; Zhong Shan Jin Qiao, ZLI-9017) for 30s and hematoxylin was used for counterstaining for 2 min. Finally, the sections were dehydrated in increasing concentrations of ethanol, cleared in xylene, and sealed.

Transmission electron microscopy (TEM)

Ovary tissues were obtained from 14-week-old mice and fixed in 2.5% glutaraldehyde at 4°C overnight. Subsequently, the tissues were rinsed three times for 10 min each in PBS. Then the ovary was transferred into 1% osmic acid. After 2 h, it was washed three times with PBS for 10 min each time. The ovaries were fixed with 2% uranyl acetate for 30 min and dehydrated in ethanol gradients (50%, 70%, 90%, and 100%) for 10 min each. Transferred to a solution of 90% acetone and 90% ethanol (1:1) for 20 min, then the samples were transferred to 90% acetone at 4°C for 20 min, followed by two transfers to 100% acetone for 15 min each. Finally, they were embedded in epoxy resin. Semi-thin sections after staining with 1% methylene blue in 0.5% borax were examined using an Olympus BX60 light microscope. And ultrathin sections (50 nm), stained by lead citrate, were observed using a HITACHI H-7650 transmission electron microscope (HITACHI, Japan).

Western blot analysis

A total of 100 oocytes were collected from each group. Each protein sample was extracted using a cell lysis solution containing 1% PMSF (Cell Signaling Technologies) following the manufacturer's instructions and protein samples underwent boiling at 100°C for 5 min. The supernatant of ovarian tissue homogenates was lysed in tissue lysis buffer on ice for 30 min and then kept at 100°C for 5 min. The proteins were subsequently separated on a 10% SDS-PAGE gel. Then, proteins were transferred to the polyvinylidene fluoride membrane (Millipore, USA) through a transmembrane transfer. Membranes were immersed in 5% skimmed milk for 2 h at room temperature, washed briefly with TBST (TBS containing 0.1% Tween 20), and incubated with primary antibodies overnight at 4°C. Rinse the membranes 3 times with TBST for 10 min, then incubate them with secondary antibody for 1 h at room temperature and rinse them 3 times with TBST for 15 min each. Finally, the signals were detected using an enhanced chemiluminescence (ECL) kit (KeyGEN BioTECH, KGC4602-200) and quantitatively analyzed in grayscale with ImageJ.

In vitro fertilization and embryo culture

Caudae epididymides from 8-week-old male mice were dissected in a dish containing HTF (Nanjing Aibei Biotechnology Co., Ltd.M1335) medium under mineral oil to release sperm. The sperm were then capacitated for 1 h at 37°C in a 5% CO2 atmosphere. MII oocytes were collected in 100μL HTF medium, and 10μL capacitated sperm was added and cultured at 37°C and 5% CO2 for 5 h. The presence of two

pronuclei indicates successful fertilization. Embryos were cultured in mineral oil-covered culture drops containing 150μL KSOM (Nanjing Aibei Biotechnology Co., Ltd.M1435) at 37°C in a 5% CO2 atmosphere, and the 2-cell formation rate was counted for 24 h.

QUANTIFICATION AND STATISTICAL ANALYSIS

The data were analyzed using GraphPad Prism 10. Each experiment included at least three independent samples and was replicated three times. The results are presented as mean ± standard error of the mean (SEM). Two-tailed unpaired Student's t-tests were used to compare the results of two experimental groups. A *p*-value of less than 0.05 was considered statistically significant.